Optimization of Sphere Population for Electrostatic Multi-Sphere Method

Daan Stevenson and Hanspeter Schaub

***Abstract*— To develop the robust relative position and orientation control algorithms for Coulomb charge control of spacecraft, accurate but computationally efficient electrostatic models are necessary. The multi-sphere method (MSM) predicts the interactions of a charged spacecraft using multiple conducting spheres. To improve the accuracy of this model further, a new method is proposed whereby equal radius spheres are placed uniformly on the surface of the spacecraft. The radius is chosen such that the MSM predicts the same self-capacitance for the conducting geometry as a numerical solution does. While similarities are identified between the new method and the established boundary element method, several key distinctions between the models are established. The accuracy of the new approach is verified using a simple system with two spheres, whereby its ability to capture-induced charge effects is highlighted. Then, a cylinder–sphere system is analyzed using 105 spheres on the cylinder and 30 spheres on the sphere, providing comparison with a previous three-sphere volume populated model for the cylinder. The surface populated model provides much higher accuracy in forces and torques when the separation distances are within 10 craft radii, but there is a little improvement outside this range. While the cylinder MSM with three spheres provides force solutions an order of magnitude quicker than the surface MSM method, the setup time for the surface populated MSM is two orders of magnitude faster.**

***Index Terms*— Charge transfer, electrostatic analysis, space vehicle control.**

I. Introduction

A SUBSTANTIAL research effort is in progress to determine the feasibility of using active Coulomb charging for relative motion control of nearby spacecraft. Using electron or ion emitters, a spacecraft can accurately control its voltage up to 10 s of kilovolt within milliseconds. If the proximity and charge on two craft are sufficient to overcome the local plasma environment, the resultant forces can be used to affect their relative position [1]–[5]. In the realm of cooperative formation flying missions, this technology provides a benefit over thruster control in its power efficiency and lack of expendable fuel or exhaust plumes. Furthermore, there are some exciting noncooperative applications for Coulomb charge control, such as electrostatic tugs used to reorbit debris objects [6]–[8].

The drawback that accompanies the benefits of electrostatic actuation is a decrease in controllability. Only one dimension of control is possible per spacecraft body while the resultant electrostatic forces and torques are dictated by the craft shapes, positions, and orientations. Moreover, real-time knowledge of the exact electrostatic interactions is not possible as there is no analytic solution to Poisson's equation for the potential fields surrounding generic geometries. There are various models that approximate the electrostatics of 3-D bodies, each presenting a compromise between accuracy and computational cost, as shown in Fig. 1. The highlighted model, which attempts to bridge the gap in accuracy between previous simplified models and finite element analysis (FEA) approaches while keeping computational costs low, is the subject of this paper.

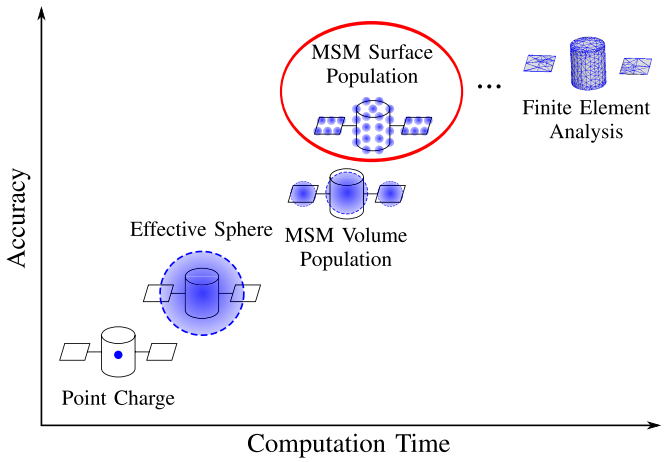

Fig. 1. Comparison of various electrostatic models.

The simplest approximation is to treat a spacecraft as a prescribed point charge. This method is used in numerous studies that analyze the relative motion dynamics of Coulomb formations [9]–[15]. While the execution of the point charge model is as simple as computing Coulomb's law, it results in a substantial approximation. In reality, charge transfer devices operate using closed-loop control on measurements of the spacecraft electric potential relative to the ambient space environment. The total electric charge is then a function of the spacecraft geometry and external potential fields, and is distributed asymmetrically across conducting surface.

An increase in accuracy can be achieved by modeling a spacecraft using an effective sphere with a radius that best represents its electrostatic interaction [16]. When multiple spacecraft is analyzed together, consideration of the position-dependent capacitance (PDC) effect improves knowledge of the voltage to charge relationship throughout the system [17]. One drawback of this approach is that it does not capture the

Manuscript received October 11, 2012; revised May 22, 2013; accepted September 21, 2013. Date of publication October 9, 2013; date of current version December 9, 2013. This work was supported by the NASA Science and Technology Research Fellowship under Grant NNX11AN47H.

The authors are with the Colorado Center for Astrodynamics Research, University of Colorado, Boulder, CO 80309-0431 USA (e-mail: daan.stevenson@colorado.edu; hanspeter.schaub@colorado.edu).

Color versions of one or more of the figures in this paper are available online at http://ieeexplore.ieee.org.

Digital Object Identifier 10.1109/TPS.2013.2283716

nonsymmetric distribution of charge within a body in small separation distances. For two identical spheres, induced charge effects can be approximated by certain analytic approaches, but these methods do not expand to multiple or varying size spheres.

Another limitation of the effective sphere method presented in [16] is its inability to resolve electrostatic torques and non line-of-sight forces that result from nonsymmetric spacecraft bodies. This is crucial when relative attitudes and small separation distances in the order of the spacecraft dimensions are a consideration in the mission scenario. The multi-sphere method (MSM), as presented in [18], is an approach that attempts to resolve these shortcomings. A generic spacecraft shape is modeled by a collection of conducting spheres. Computation is limited to inverting an $n \times n$ matrix (where n is the number of spheres in the system) to determine the charge on each sphere, and forces and torques are subsequently predicted by summation of the contribution of each sphere by Coulomb's law. This allows for six degree of freedom electrostatic simulations of relative spacecraft motion in real time, which is crucial for the development of robust relative position and orientation control algorithms in local space situational awareness applications.

At the most accurate end of the spectrum, FEA software such as ANSOFT's Maxwell3D, [19] creates a highly precise but computationally expensive solution of the electrostatic potential fields by solving Poisson's equation on each finite element in the entire 3-D space, with boundary conditions created from the spacecraft geometries and potentials. FEA solvers are not capable of faster than real-time charged relative motion simulations, and therefore do not provide analytical insight into the dynamics and control of such scenarios. They are, however, useful for creating truth solutions that can be used to verify the lower order models of interest here.

The prior MSM scheme that populates the spacecraft volume with interior spheres is referred to as the volume MSM (VMSM). Here, a nonlinear fit is used to match the forces and torques from a truth model, as described above, at various separation distances and orientations. One drawback of this VMSM approach is the necessity for an external shape to generate forces and torques. Another limitation is that, despite implementing symmetry arguments, the nonlinear fit is not robust for increasing numbers of spheres, which is desirable to capture the 3-D and induced charge effects of more intricate geometries at small separation distances. This paper will investigate how to populate generic spacecraft shapes with higher numbers of uniformly positioned spheres, placed on the surface of the conducting body. This method is referred to as the surface MSM (SMSM). There is a slightly higher computational cost when computing forces and torques due to the increase in size of the PDC matrix, but the time necessary to setup the model is dramatically decreased. In the end, this new method helps to bridge the gap in accuracy between the original MSM and FEA approaches. Meanwhile, none of the models discussed above are rendered obsolete by the inclusion of a new approach, if the tradeoffs of computation time and accuracy are considered. Rather, the SMSM method provides a new tool for scenarios where increased accuracy

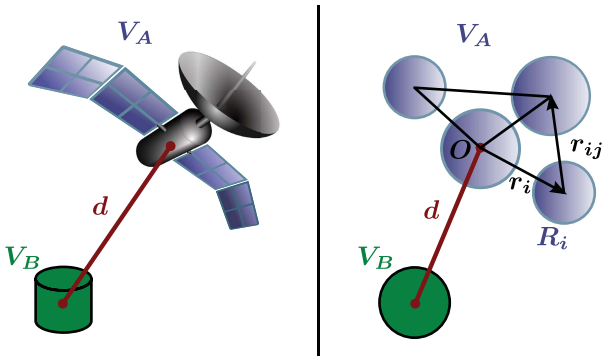

Fig. 2. Conceptual depiction of MSM.

electrostatic force and torque modeling are critical because separation distances are in the order of craft radii.

II. MSM Review

To discuss the new method for populating spheres on the surface of a spacecraft body, the general MSM is reviewed. The novel SMSM research addresses how the size and location of spheres are chosen. Once this is accomplished, computing forces and torques on the bodies in the system are equivalent to the original methodology proposed in [18]. A rigid spacecraft or space debris object is modeled by a collection of spheres with fixed sizes and relative positions, as shown in Fig. 2. Satellite A is modeled by four spheres, whereas object B happens to be represented by a single sphere.

While the absolute electrostatic voltage is assumed to be prescribed on a spacecraft, the Coulomb force between the spheres depends on the total charge that each holds. The voltage V_i on a given sphere is a result of both the charge on that sphere and the charges on its neighboring spheres. This relation is given in (1), [17], and [20] where R_i is the radius of the sphere in question and $\boldsymbol{r}_{i,j} = \boldsymbol{r}_j - \boldsymbol{r}_i$ is the center-to-center distance to each neighbor. The constant $k_c = 8.99 \times 10^9$ Nm^2/C^2 is Coulomb's constant, and q_i is the charge on a given sphere

$$V_i = k_c \frac{q_i}{R_i} + \sum_{j=1, j\neq i}^{m} k_c \frac{q_j}{r_{i,j}}. \tag{1}$$

The linear relations for each of the $m = n + 1$ spheres in the system (n spheres in the MSM plus the external sphere) can be combined in the matrix form of (2), where $\boldsymbol{V} = [V_A, V_A, \ldots, V_A, V_B]^T$ and $\boldsymbol{q} = [q_1, q_2, \ldots, q_n, q_B]^T$ are matrix collections of the voltages and charges in the entire system

$$\boldsymbol{V} = [C_M]^{-1}\boldsymbol{q}. \tag{2}$$

Note that V_A is the prescribed voltage on all spheres in the model while the external sphere is held at V_B. The effect of varying the voltage on different spheres within the model has not been analyzed, but keeping the voltage constant is logical since the modeled conducting spacecraft would be held at uniform voltage. This approach also reduces the amount of model parameters.

The inverse of the PDC matrix in (2), $[C_M]^{-1}$, can be expanded as follows, according to the nomenclature adopted in Fig. 2, with $\boldsymbol{r}_{i,B} = \boldsymbol{d} - \boldsymbol{r}_i$

$$[C_M]^{-1} = k_c \begin{bmatrix} 1/R_1 & 1/r_{1,2} & \cdots & 1/r_{1,n} & 1/r_{1,B} \\ 1/r_{2,1} & 1/R_2 & \ddots & \vdots & \vdots \\ \vdots & \ddots & \ddots & \vdots & \vdots \\ 1/r_{n,1} & \cdots & \cdots & 1/R_n & 1/r_{n,B} \\ 1/r_{B,1} & \cdots & \cdots & 1/r_{B,n} & 1/R_B \end{bmatrix}. \tag{3}$$

The next step is to solve for the array of charges $\boldsymbol{q}$ from (2) by inverting this $n+1$ size symmetric matrix, a computation that becomes increasingly intensive when more spheres are used in the model. Coulomb's law can then be implemented to calculate the linear force between each charged sphere. Since the location of the spheres within the modeled body are held fixed with respect to each other, their equal and opposite contributions cancel. The total force $\boldsymbol{F}$ and torque $\boldsymbol{L}$ about the origin O on body A due to external shape B is then given by the following summations:

$$\boldsymbol{F}_O = k_c q_B \sum_{i=1}^{n} \frac{q_i}{{r_{i,B}}^3} \boldsymbol{r}_{i,B} \tag{4}$$

$$\boldsymbol{L}_O = k_c q_B \sum_{i=1}^{n} \frac{q_i}{{r_{i,B}}^3} \boldsymbol{r}_i \times \boldsymbol{r}_{i,B}. \tag{5}$$

While any origin can be chosen for body A, the force and torque in (4) and (5) are now defined from this reference origin. If the object B is modeled by another MSM, the force and torque relations contain double summations.

III. Surface Population Motivation

During previous developments, three spheres are used to model a cylinder shape. While considering symmetry of the original geometry, the optimal size and position of each sphere are determined by fitting to the numerically solved force and torque values on the cylinder in the presence of a charged external sphere. While this volume-based sphere population works well to predict the electrostatic interactions of the cylinder shape, capturing the 3-D and induced charge effects of more intricate geometries at small separation distances requires a model with more than three spheres. The MSM algorithm for calculating forces and torques can handle models with large numbers of spheres, but the nonlinear fitting schemes used to optimize the sphere positions and sizes are not robust in this domain. As with any nonlinear fitting algorithm, when the parameter set increases, successful convergence is dependent on the chosen initial conditions and global optimization is not guaranteed.

Due to the limitations of the nonlinear fit, expanding the MSM to higher accuracy levels requires populating the spacecraft shape with an increasing number of uniformly positioned spheres. This leads to a higher fidelity prediction of the electrostatic interactions because there is more freedom for redistribution of the charge between the various spheres in the model as relative orientations change, much like there is on the surface of an actual conducting object. In this way, induced charge effects can be captured in any dimension where multiple spheres are present. Since the underlying assumption that the modeled body is fully conducting remains, it is known that all the contained charge will reside on its surface. Therefore, the approach is taken to populate only the surface of a given shape with spheres.

The goal of the new method of surface population is to minimize the parameters that need to be selected when creating an MSM for a given shape. Therefore, it is desirable to pick a set of spheres that are uniformly distributed along the surface of the geometry. For complex shapes, this is not a trivial task. Several CAD programs contain algorithms to generate point clouds from solid models and this is most likely the approach that will be taken during future work for generating sphere positions for generic spacecraft. For simpler shapes, such as spheres and cylinders, specific algorithms are created to uniformly populate the surface as described as follows. By this approach, the new SMSM method is significantly faster and more robust to setup than the VMSM. The resulting computations are more accurate, while the runtime costs are only marginally increased.

IV. Two-Sphere System

To analyze the quality of a uniform surface populated MSM, simple shapes are used to provide benchmark performance results. An analytic solution exists for the self-capacitance of an isolated sphere in space, and for a system with two spheres separated at appreciable distances the PDC model can predict Coulomb forces fairly accurately. For smaller separation distances, in which case the charge is not uniformly distributed along the surface of each sphere, several numerical and approximate analytic options exist that can be used as accurate truth models. By comparing these truth models with the PDC solution, it is easy to isolate the specific contribution from induced charge effects.

A. Uniform Population on a Sphere

To model the two-sphere system with the MSM, the goal is to uniformly populate the surface of a sphere with equidistant points, which is a well-documented computer science problem [21]. Coincidentally, the most robust algorithms involve equal electrostatic repulsion of the points, which could be used to generate surface points for generic shapes in later research. For the current effort, a golden section spiral distribution provides sufficiently uniform spacing of points. The spiral divides the sphere into parallel bands of equal width, and points are placed along the spiral at successive longitudes separated by the golden angle

$$\psi = \pi \left(3 - \sqrt{5}\right). \tag{6}$$

Fig. 3 shows the resulting sphere population for $n = 4,\ 10,$ and 30 spheres.

B. Optimal Packing Parameter

With the spheres in the MSM positioned in a uniform manner on the surface of the modeled geometry, the one

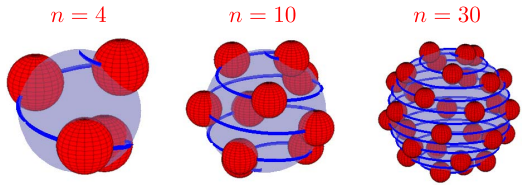

Fig. 3. Various uniform point distributions on the surface of a sphere.

remaining parameter to choose is the spheres' radii R, which are assumed constant throughout the SMSM model. While the goal is ultimately to match Coulomb forces and torques with external objects, only one scalar invariant quantity is necessary to determine an optimal radius. In contrast to the VMSM method where increasing numbers of sphere locations and radii must be chosen as the number of spheres increases, the SMSM method only needs to determine a single parameter R once uniform positions are chosen. This provides a significant simplification of the model development with a large number of spheres. The self-capacitance of an isolated conductor is dependent only on its geometry, and is therefore a good candidate scalar quantity for determining the optimal sphere radius R.

For a modeled sphere with radius R_S, the self-capacitance C is analytically known

$$C_{\text{sphere}} = \frac{R_S}{k_c}. \tag{7}$$

Meanwhile, the capacitance of the MSM can be computed by summation of the charge q_i on each sphere in the model (as determined by the process in Section II) for a given voltage V

$$C_{\text{MSM}} = \frac{Q}{V} = \frac{\sum_{i=1}^{n} q_i}{V}. \tag{8}$$

A simple optimizing function based on a golden section search and parabolic interpolation is used to choose a radius R that minimizes

$$f(R) = C_{\text{MSM}} - C_{\text{sphere}}. \tag{9}$$

This is performed for various n numbers of spheres in the model.

To analyze the optimal sphere size across various geometries, comparing the total surface area $4\pi R^2 n$ of every sphere in the MSM to the total surface area S of the modeled geometry provides geometric insight. This relation is represented by the packing parameter γ

$$\gamma = \frac{4\pi R^2 n}{S}. \tag{10}$$

For the benchmark spherical spacecraft case being modeled with the SMSM, the optimal packing parameter is plotted against the number of spheres in the model in Fig. 4. Interestingly, even though the number of spheres in the model and therefore the spacing between them changes, the parameter γ appears to converge to a constant value.

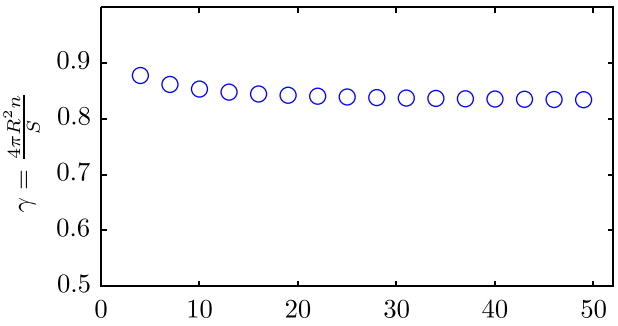

Fig. 4. Optimal packing parameter for surface MSM on sphere.

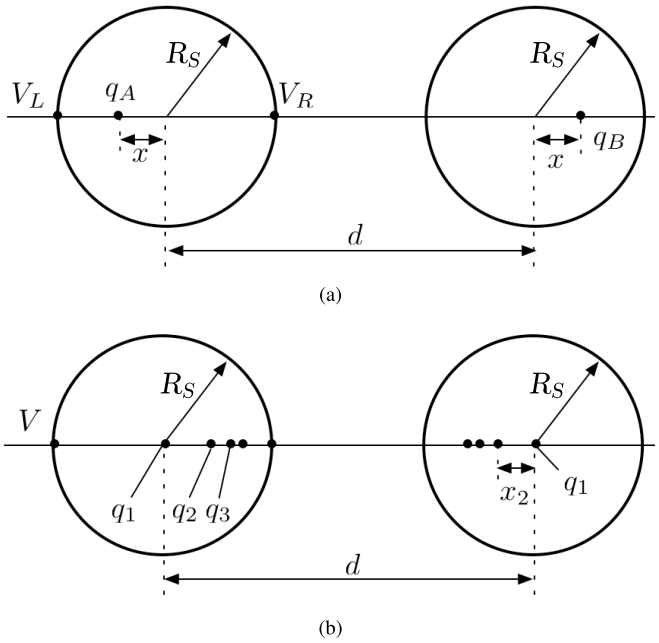

Fig. 5. Two analytic models for the two-sphere system that capture induced effects. (a) First-order induced charge model (repulsion). (b) Electrostatic MOIs.

C. Truth Models

While the radii of the spheres in the model are optimized as above to match the self-capacitance of the modeled sphere, validation requires that the resultant electrostatic forces match those from numerical and series summation solutions. A simple system is used that consists of two spheres with radii $R_S = 0.5$ m, various separation distances d, and equal as well as opposite sphere voltages $V = \pm 30$ kV.

The simplicity of the two-sphere system lends itself to several approximate analytic solutions where more complex systems do not. The PDC model for two spheres captures the relationship between the prescribed voltage and the total charge on each sphere, but not the induced charge effects. If each sphere is modeled with a single charge at its center, the resulting voltage in space is not constant at the sphere boundaries, as it would be on a conducting body. The two approaches in Fig. 5 attempt to offset this anomaly by ensuring that the spheres form equipotential surfaces. They are valid only for a system where both conducting spheres are of equal radius and are held at equal magnitude voltages, as is the case here.

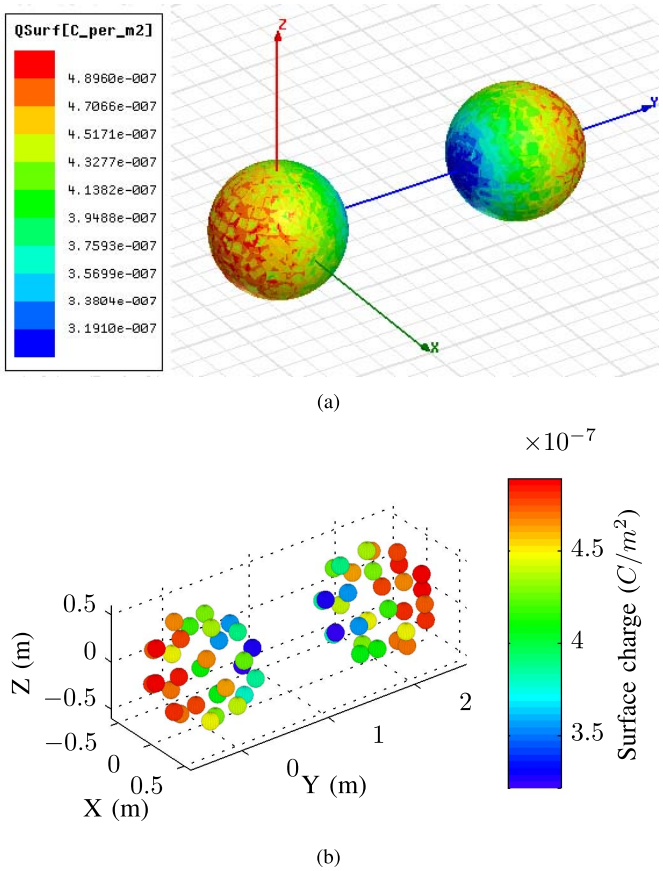

Fig. 6. Charge density distribution on two spheres ($V_1 = V_2 = +30$ kV). (a) Maxwell3D. (b) MSM with 30 spheres.

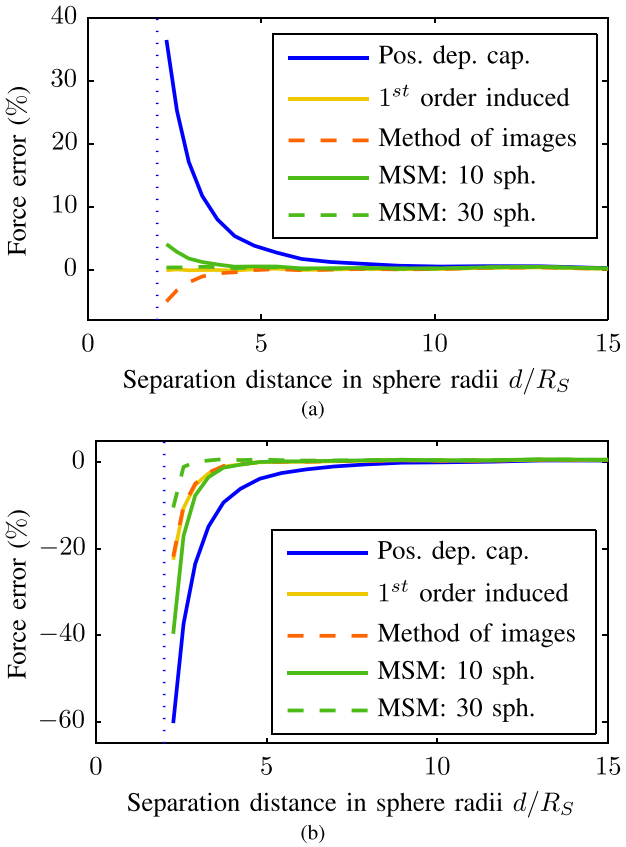

Fig. 7. Error in force between two spheres for various electrostatic models. (a) Repulsive forces ($V_1 = +30$ kV, $V_2 = -30$ kV). (b) Attractive forces ($V_1 = V_2 = +30$ kV).

The first-order induced charge model, shown in Fig. 5(a), attempts to capture-induced effects by a 1-D change in separation distances. The separation d between the charges q_A and q_B that are computed using the PDC matrix, is adjusted by an extra distance x. This distance is chosen such that V_L and V_R are equal, resulting in a cubic equation in x [22]. The figure shows an increased separation as for the repulsion case; attraction would result in a decreased separation distance.

In Soules' method of images (MOI), shown in Fig. 5(b), successively smaller image charges q_i are placed at distances x_i along the line of centers to approximate the induced charged distribution [23]

$$q_i = \pm \frac{r q_{n-1}}{d - x_{n-1}} \tag{11a}$$

$$x_i = \frac{{R_S}^2}{d - x_{n-1}}. \tag{11b}$$

Here $n > 1$, q_1 is determined for a given voltage using the PDC model, and $x_1 = 0$. In (11b), the successive charges switch polarity $(-)$ for the repulsion case and maintain the same polarity $(+)$ for attraction [20]. The algorithm is implemented using 19 spheres as in [22].

While the two-induced charge models discussed above provide a vast improvement over the PDC model in force prediction at small separation distances, Maxwell3D is found to produce the most accurate solution when the simulation is tuned properly. Therefore, the Maxwell3D solution is used as the truth model for verification of the surface populated MSM. The mesh and charge distribution are visible in Fig. 6(a).

D. Force Comparison

Fig. 6 shows the charge density distribution in both Maxwell3D and on a 30-sphere surface populated MSM. This qualitatively highlights the ability of the SMSM to capture induced charge effects when enough spheres are present on the object surface. To offset the difference in surface areas, the charge density σ_i on each sphere in Fig. 6(b) is normalized by the factor γ from (10)

$$\sigma_i = \gamma \frac{q_i}{4\pi {R_i}^2}. \tag{12}$$

Radii for the models are chosen to fit capacitance of the sphere, as discussed above, resulting in

$$R \text{ (10 spheres)} = 0.1460 \text{ m} \tag{13}$$

$$R \text{ (30 spheres)} = 0.0835 \text{ m}. \tag{14}$$

Fig. 7 shows the percent error for various models at a range of separation distances, for the attractive and repulsive cases [Fig. 7(a) and (b), respectively]. Percent error is defined as follows:

$$\text{Err} = \frac{F_{\text{model}} - F_{\text{Maxwell}}}{F_{\text{Maxwell}}}. \tag{15}$$

The PDC model produces almost 50% error at very small separation distances, but matches the full solution well at further distances. While the Maxwell3D solution is used as the truth model, the slight disagreement with the MOIs solution is surprising, since this approach should closely represent the full series solution according to [20]. As more spheres are added to the MSM, however, the errors at close distances converge to zero, thus giving further credence to the solution given by Maxwell3D. The first-order induced charge method matches Maxwell3D for the repulsion case but is equivalent to the MOIs for the attractive case, which is likely a coincidence.

The SMSM with 30 spheres results in less than a percent error for repulsion right up to where the spheres touch at $d = 2R_S$. For attraction, induced effects are known to be even more dominant, and more spheres are necessary to completely capture these effects. The PDC model shows nearly twice as much error as for the repulsion case. The 10-sphere SMSM results in up to 40% error as the spheres nearly touch, but this drops off quickly to less than 2% when $d = 3.5R_S$. All in all, the surface populated MSM is clearly shown to model the electrostatic interactions of the spheres to a very high degree of accuracy. It provides a more accurate solution than other induced charge effect models, while increasing in accuracy as more spheres are added. Moreover, this method is expandable to generic spacecraft shapes where the others are not.

These results beg the question, how does the uniform sphere radius R, and thus the packing parameter $\gamma = 4\pi R^2 n/S$, affect the resulting force computations? In Fig. 7, this parameter is optimized such that the capacitance of the MSM matches the capacitance of the sphere that it is intended to model. If a different R is chosen, might the model match the true forces better at close separation distances? Fig. 8 shows the error in force at three separation distances, for a range of γ values, comparing both the 10- and 30-sphere models. The repulsion configuration is chosen with $V_1 = V_2 = +30$ kV.

At the larger separation distance ($d = 15R_S$), the force error is minimized when $\gamma = 0.8464$ for $n = 10$ and when $\gamma = 0.8273$ for $n = 30$, as shown by the red circle. This corresponds within a fraction of a percent to the optimal values in Fig. 4, suggesting that fitting the model-sphere radii to the body capacitance results in the optimal force prediction at larger separation distances. To match the induced charge effects and forces at closer distances, the optimal packing parameter γ (and therefore R) is smaller. Choosing R on this basis, however, would result in significant errors at larger separation distances. In the end, spacecraft proximity missions would rarely operate at fewer than 10 craft radii separation unless docking is considered, so the best approach is to choose the sphere radii by matching to the spacecraft body's self-capacitance in deep space, as outlined in Section IV-B. Notice that the sensitivity in force error to γ is appreciably decreased for the model with more spheres, which is a promising feature of the new method.

V. Surface MSM Methodology for Generic Spacecraft Shape

With the accuracy of the new model sufficiently verified for simple shapes, it can be applied to model spacecraft

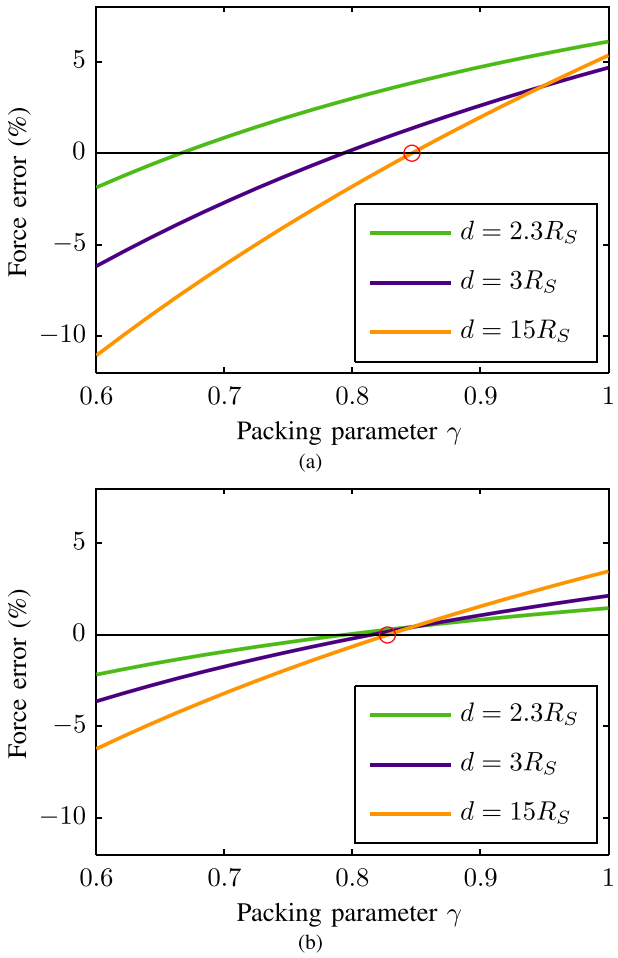

Fig. 8. Error in force for various packing parameters. MSM with (a) 10 and (b) 30 spheres.

with arbitrary 3-D shapes. Before the results for such shapes are analyzed, the methodology for determining the sphere parameters for a generic spacecraft shape is shown in Fig. 9. The red boxes are the processes that must be executed when analytic solutions are not present for the sphere distribution and capacitance, as is most often the case. The two components of a full MSM are the location $\boldsymbol{r_i}$ and radius R_i of each sphere. For a generic body, a solid modeling program will be necessary to determine a uniform point cloud model on the surface. For most shapes, the capacitance is to be found by an electrostatic modeling program such as Maxwell3D. The PDC matrix is then used to calculate the capacitance for the system of spheres to determine an optimal uniform radius R that matches the capacitance from the numerical solution. At this point, the full model can be used in conjunction with other MSM objects to determine the electrostatic interactions.

VI. Boundary Element Method

Comparison with higher order numerical solutions in this paper has been focused predominantly on finite element methods that solves Laplace's equation $\nabla^2\phi(\boldsymbol{x}) = 0$ on the free space domain outside the conducting bodies. While this numerical approach is capable of providing very high accuracy solution, the boundary element method (BEM) [24]–[27]

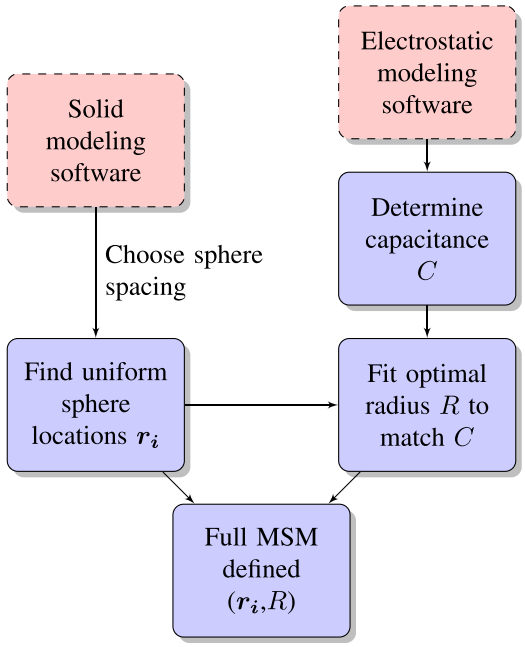

Fig. 9. Methodology for parameter selection of surface populated MSM.

is another method with considerable similarities in its mathematical formulation to the SMSM. The BEM differs from FEA in that unknowns are solved on the boundary of the domain, i.e., on the surface of conducting elements, not unlike the SMSM.

Applying Green's function to Laplace's equation on some surface S with normal n results in [24]

$$\phi(\boldsymbol{x}) = \int_S \left[G(\boldsymbol{x}, \boldsymbol{x}') \frac{\partial \phi}{\partial n}(\boldsymbol{x}') - \frac{\partial G}{\partial n}(\boldsymbol{x}, \boldsymbol{x}') \phi(\boldsymbol{x}') \right] dS(\boldsymbol{x}') \quad (16)$$

where the Green's function G for the Laplacian in 3-D is

$$G(\boldsymbol{x}, \boldsymbol{x}') = \frac{1}{4\pi |\boldsymbol{x}' - \boldsymbol{x}|}. \quad (17)$$

At this point the boundary of the domain is discretized using a set of basic functions to obtain a solution of the charge distribution σ [which is manifested in (16), in the $\partial\phi/\partial n(\boldsymbol{x}')$ term]. If Neumann boundary conditions are prescribed on the entire boundary, the second term in the integral in (16) disappears and this relation can be discretized to the following matrix form:

$$A\boldsymbol{\lambda} = \boldsymbol{b} \quad (18)$$

where $\boldsymbol{\lambda}$ contains charge distribution (σ) values on the elements and $\boldsymbol{b}$ is a column with the resulting surface voltage ϕ on a central point at each element. The matrix A is populated with analytic solutions to the following integral that results from (16) for every combination of two surface elements:

$$\phi(\boldsymbol{x}) = \int_S \frac{\sigma(\boldsymbol{x}')}{4\pi\epsilon |\boldsymbol{x} - \boldsymbol{x}'|} dS(\boldsymbol{x}'). \quad (19)$$

The formulation is similar to the capacitance matrix of the MSM, but if complex basic functions are used in the BEM, populating A becomes tedious and time consuming, in which case the SMSM provides a much simpler approach.

In its simplest form, the BEM can be implemented using the following simplifications [25].

1) Within each element, assume the charge density has a constant value so that σ is piecewise constant over the surface.
2) Use a centroidal approximation with the charge in the adjacent element concentrated at a center point in the patch to solve (19).

In this case, the off-axis terms in the matrix A simplify to $k_c/r_{i,j}$ as in the MSM capacitance matrix, while equating (19) for the self-terms (diagonal elements of the matrix) results in a geometry-dependent constant. This constant is analogous to the sphere size chosen in the SMSM.

Considering this simplified form of the BEM, the two methods require the same $O(N^2)$ inversion operation to solve for a set of charges on the boundary of the system, but some fundamental differences remain. First, setup in the SMSM is simpler because the self-integral for various element geometries (which can be computationally intensive for curved elements) is omitted; instead, a constant sphere size is determined from the single free space capacitance value used from a truth model. Further, if so desired, selection of sphere placement and size in the SMSM can be tuned to capture certain electrostatic characteristics, where the BEM is limited to a set of surface elements that span the entire boundary but do not overlap. This is an especially important distinction when considering sharp edge and corner features. In this case, spheres in the SMSM can be placed exactly along or on such features where the charge is expected to be highest, thus capturing the charge concentration at the right location. The BEM meanwhile, even if the mesh is discretized to be denser at such locations, is limited to elements that border the sharp feature rather than being located on it. This benefit of the SMSM is especially evident when a relatively small number of sphere/elements are used to capture the charge distribution on a given body. The surface populated BEM, for example, could not capture off-axis forces and torques on a cylinder using only three elements, as is possible with the MSM [18].

VII. Cylinder Model Results

A. Setup

In [18], where the MSM was first introduced, the interaction between a 3-m length by 1-m diameter cylinder and a 1-m diameter sphere is used to determine optimal sphere parameters and verify the model. Collecting force and torque values at various separation distances and orientations provide invaluable insight into the ability of a model to replicate-induced charge effects, 3-D effects, and large distance behaviors. The same approach is implemented to verify the surface populated MSM and compare it with the three-sphere model from the previous research. Using a set of Maxwell3D data that ranges from cylinder–sphere contact to 20-m separation distance, the model in Fig. 10 is generated, with parameters listed in Table I. Note that in comparison with the setup shown in Fig. 9, choosing parameters for this three-sphere model necessitates

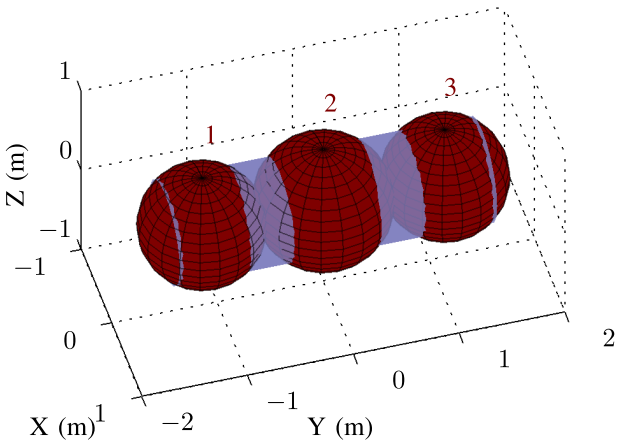

Fig. 10. MSM parameters for cylinder geometry.

TABLE I
PARAMETERS OF THREE-SPHERE MSM FOR CYLINDER

	Sphere 1	Sphere 2	Sphere 3
X Coordinate (m)	0	0	0
Y Coordinate (m)	-1.1454	0	1.1454
Z Coordinate (m)	0	0	0
Radius (m)	0.5959	0.6534	0.5959

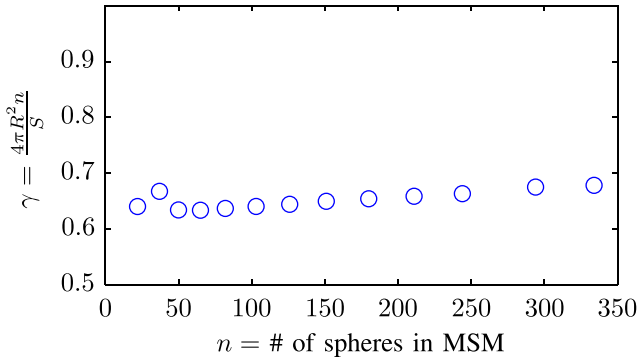

Fig. 11. Optimal packing parameter for surface MSM on cylinder.

collecting a full sweep of Maxwell3D truth data, followed by a difficulty to implement nonlinear fit.

Now, the methodology in Fig. 9 is implemented. Since the cylinder is still a fairly simple shape, manual algorithms are used to populate the surface. For the end discs, a gold section spiral is used much likely for populating the spheres in Fig. 3, while on the circumference of the body, hexagonal packing is implemented. Maxwell3D is used to determine that the self-capacitance of the cylinder in space is

$$C_{\text{cylinder}} = 1.0616 \times 10^{-10} \frac{C}{V}. \tag{20}$$

This is used to fit the optimal sphere radius, resulting in Fig. 11, which shows the packing parameter γ as a function of the total number of spheres n in the cylinder model. Clearly, the optimal γ values do not match those for the sphere in Fig. 4. For this reason, R must be fit for a specific sphere distribution to match the capacitance of a given model shape.

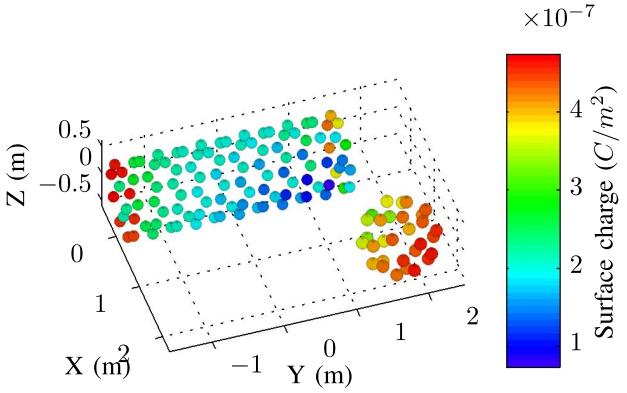

Fig. 12. Charge density distribution on SMSM of cylinder and sphere ($V_1 = V_2 = +30$ kV).

A cylinder model with $n = 105$ spheres ($R = 0.0731$ m) and a sphere model with $n = 30$ spheres as above ($R = 0.0835$ m) is shown in Fig. 12. Each is held at $V = +30$ kV and the induced charge effects are clearly visible from the charge distribution throughout the shapes.

B. Results

Figs. 13 and 14 show the accuracy of the force and torque, respectively, calculated by the VMSM model with three spheres and the surface populated model (105 spheres in the cylinder and 30 spheres in the sphere), compared with the truth data from Maxwell3D. Fig. 13(a) shows a 1–1 plot between the MSM models and the Maxwell3D data, where the black line represents perfect matching between the two models. The three-sphere VMSM overpredicts the larger forces that correspond to small separation distances. The drawback of this visualization is that it is not possible to see where in relation to the cylinder the sphere is located for a given data point. Fig. 13(b) and (c) rectifies this shortcoming, as they show the absolute force errors compared with Maxwell3D, for the three-sphere and surface-populated MSM, respectively. A representative size cylinder and sphere are included for reference, while the color legend is in logarithmic scale. The same organization is used in Fig. 14 for the torques exerted on the cylinder.

It is clear from the figures that the SMSM predicts the forces much better at small separation distances across the range of angles, but by about 6 m separation (12 craft radii), the difference between the two models is fairly negligible. For the case of torques, the three-sphere model actually does a slightly better job at separation distances larger than 4 m (eight craft radii). This is likely because the volume populated model is fit directly to the Maxwell3D data, which has been shown earlier to exhibit some accuracy discrepancies at this range. Regardless, most Coulomb charge control applications that do not involve docking occur at separation distances beyond this range.

It is important to weigh the accuracy with computation and setup times of the different models, as listed in Table II. The first column gives the time for each model to compute a force and torque value at each of the 82 relative positions.

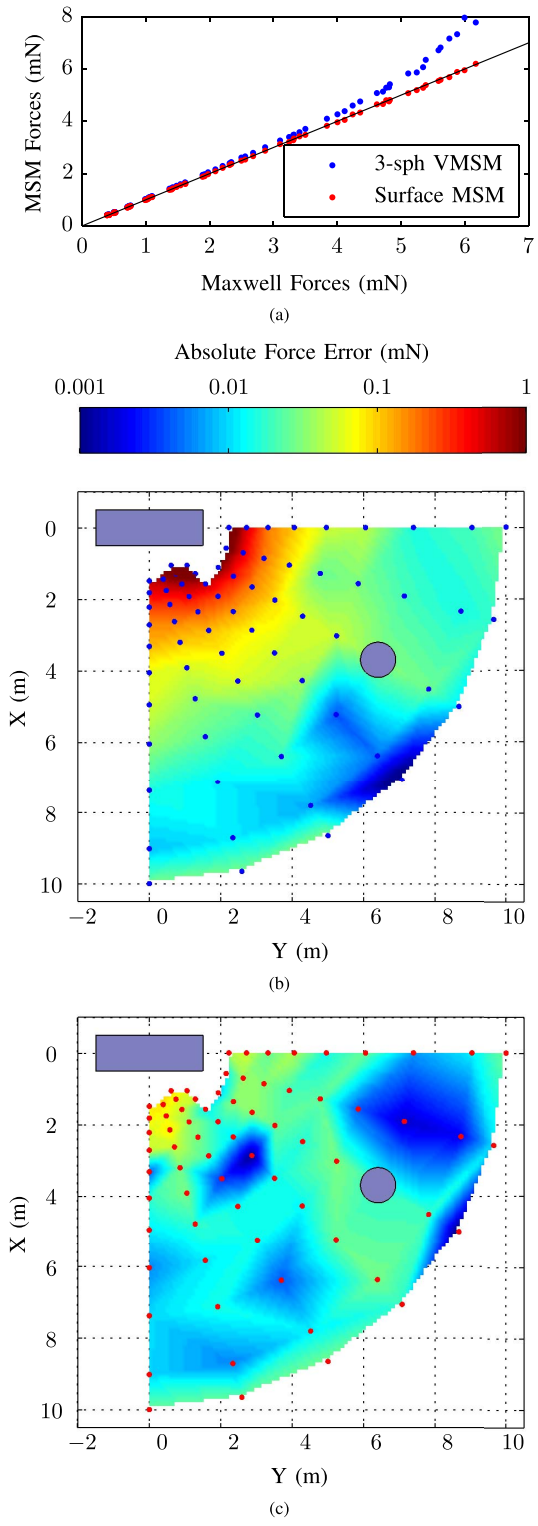

Fig. 13. Force comparison between MSM models and Maxwell3D. (a) Both models compared with Maxwell3D. (b) Three-sphere VMSM errors. (c) Surface MSM errors.

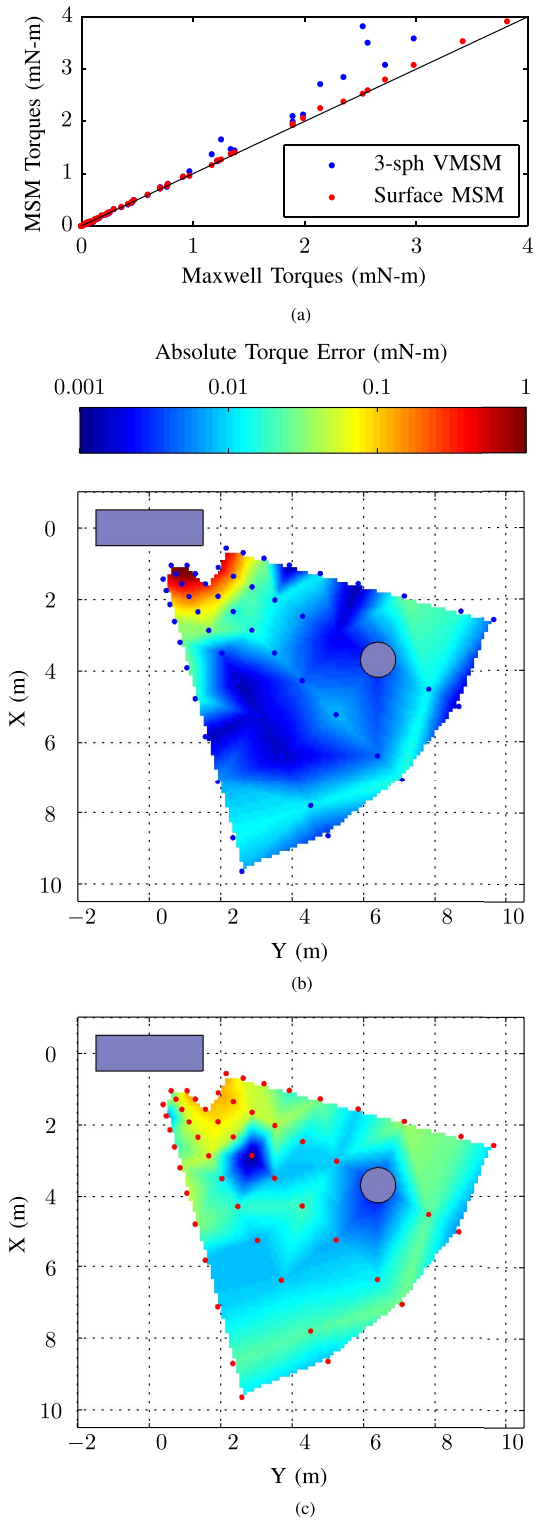

Fig. 14. Torque comparison between MSM models and Maxwell3D. (a) Both models compared with Maxwell3D. (b) Three-sphere VMSM errors. (c) Surface MSM errors.

While this computation takes Maxwell3D about 1 h and 14 min at fairly moderate accuracy settings, the MSM with three spheres completes the task in a fraction of a second. Meanwhile, it takes the surface populated model (with 135 spheres in the system) about 16 s. The next column shows the numerical calculation time necessary for the setup of the two MSM models. For the volume populated (three spheres) MSM, this requires the complete set of data calculated earlier by Maxwell3D, while the surface populated MSM only requires a single numerical computation of the capacitance of

TABLE II
SETUP AND COMPUTATION TIME FOR CALCULATION OF FORCE AND TORQUES BETWEEN SPHERE AND CYLINDER AT 82 RELATIVE LOCATIONS

[Time in sec]	Comp.	Setup				
Maxwell3D	4434	Num.		Fit		Total
3-sph VMSM	**0.11**	4434	+	9.1	=	**4443.1**
Surface MSM	**15.6**	54.1	+	4.1	=	**58.2**

the body. The fit column represents the nonlinear numerical fit for the three-sphere VMSM, and determination of the sphere positions as well as a fit to match R to capacitance for the surface populated model. As is clear, computation happens about an order of magnitude quicker for the VMSM, but setup is two orders of magnitude quicker for the new model. Depending on the requirements on accuracy and computation time, both models are viable candidates for use in the calculation of spacecraft electrostatic interactions. Both exceed Maxwell3D or other FEA software in the ability to predict forces and torques in real time.

VIII. CONCLUSION

In an attempt to increase the accuracy of the MSM while avoiding the complicated nonlinear parameter fit, a new surface sphere population method is created. Spheres are uniformly placed on the surface of a modeled spacecraft shape, while the common sphere radius is chosen to match the numerically determined capacitance of the conducting object. This greatly reduces the setup time for the MSM (by two orders of magnitude), while the computation time is slightly increased due to the larger number of spheres (one order of magnitude). The result is a model that captures small separation distance-induced charge effects very successfully, nearing the accuracy in electrostatic force and torque calculation of a full FEA solution. Initial verification is performed using a simple system with two spheres, for which numerical and approximate analytical solutions are available as truth models. The surface populated MSM converges to a full FEA solution for increasing numbers of spheres, even as separation distances become especially small. Next, forces and torques on a cylinder are examined, showing that the increase in spheres from the three-sphere MSM to a 105-sphere surface MSM results in a vast improvement in accuracy up to about 10 craft radii separation distance, outside of which both models perform equally well.

REFERENCES

[1] L. B. King, G. G. Parker, S. Deshmukh, and J.-H. Chong, "Spacecraft formation-flying using inter-vehicle coulomb forces," NASA/NIAC, Washington, DC, USA, Tech. Rep., Jan. 2002, http://www.niac.usra.edu/files/studies/final_report/601King.pdf.

[2] L. B. King, G. G. Parker, S. Deshmukh, and J.-H. Chong, "Study of interspacecraft coulomb forces and implications for formation flying," *AIAA J. Propuls. Power*, vol. 19, no. 3, pp. 497–505, May/Jun. 2003.

[3] H. Schaub, G. G. Parker, and L. B. King, "Challenges and prospect of coulomb formations," *J. Astron. Sci.*, vol. 52, nos. 1–2, pp. 169–193, Jan./Jun. 2004.

[4] A. C. Tribble, *The Space Environment—Implications for Spacecraft Design*. Princeton, NJ, USA: Princeton Univ. Press, 2003.

[5] M. H. Denton, M. F. Thomsen, H. Korth, S. Lynch, J. C. Zhang, and M. W. Liemohn, "Bulk plasma properties at geosynchronous orbit," *J. Geophys. Res.*, vol. 110, no. A7, pp. 1–17, Jul. 2005.

[6] H. Schaub and D. F. Moorer, "Geosynchronous large debris reorbiter: Challenges and prospects," in *Proc. AAS Kyle T. Alfriend Astrodyn. Symp.*, Monterey, CA, USA, May 2010, no. AAS 10-311, pp. 1–16.

[7] H. Schaub and L. E. Z. Jasper, "Circular orbit radius control using electrostatic actuation for 2-craft configurations," in *Proc. AAS/AIAA Astrodyn. Specialist Conf.*, Girdwood, AK, USA, Jul./Aug. 2011, no. AAS 11–498, pp. 1–17.

[8] E. Hogan and H. Schaub, "Relative motion control for two-spacecraft electrostatic orbit corrections," in *Proc. AAS/AIAA Spaceflight Mech. Meeting*, Girdwood, AK, USA, Jul./Aug. 2011, no. AAS 11–466, pp. 1–20.

[9] J. Berryman and H. Schaub, "Analytical charge analysis for 2- and 3-craft coulomb formations," *AIAA J. Guid., Control, Dyn.*, vol. 30, no. 6, pp. 1701–1710, Nov./Dec. 2007.

[10] H. Vasavada and H. Schaub, "Analytic solutions for equal mass four-craft static coulomb formation," *J. Astron. Sci.*, vol. 56, no. 1, pp. 17–40, Jan./Mar. 2008.

[11] E. Hogan and H. Schaub, "Collinear invariant shapes for three-craft coulomb formations," *Acta Astron.*, vol. 12, pp. 78–89, Mar./Apr. 2012.

[12] G. G. Parker, C. E. Passerello, and H. Schaub, "Static formation control using interspacecraft coulomb forces," in *Proc. 2nd Int. Symp. Format. Flying Missions Technol.*, Washington, DC, USA, Sep. 2004.

[13] H. Schaub, C. Hall, and J. Berryman, "Necessary conditions for circularly-restricted static coulomb formations," *J. Astron. Sci.*, vol. 54, nos. 3–4, pp. 525–541, Jul./Dec. 2006.

[14] H. Schaub, "Stabilization of satellite motion relative to a coulomb spacecraft formation," *J. Guid., Control Dyn.*, vol. 28, no. 6, pp. 1231–1239, Nov./Dec. 2005.

[15] A. Natarajan and H. Schaub, "Linear dynamics and stability analysis of a coulomb tether formation," *J. Guid., Control, Dyn.*, vol. 29, no. 4, pp. 831–839, Jul./Aug. 2006.

[16] L. E. Z. Jasper and H. Schaub, "Effective sphere modeling for electrostatic forces on a three-dimensional spacecraft shape," in *Proc. AAS/AIAA Spaceflight Mech. Meeting*, Girdwood, AK, USA, Jul./Aug. 2011, no. AAS 11–465, pp. 1–19.

[17] W. R. Smythe, *Static and Dynamic Electricity*, 3rd ed. New York, NY, USA: McGraw-Hill, 1968.

[18] D. Stevenson and H. Schaub, "Multi sphere modeling for electrostatic forces on three-dimensional spacecraft shapes," in *Proc. AAS/AIAA Spaceflight Mech. Meeting*, Charleston, SC, USA, Jan./Feb. 2012, no. AAS 12-106, pp. 1–18.

[19] ANSYS. (2010). *Maxwell 3D Software*, Sheffield, U.K. [Online]. Available: http://www.ansoft.com/products/em/maxwell

[20] J. Sliško and R. A. Brito-Orta, "On approximate formulas for the electrostatic force between two conducting spheres," *Amer. J. Phys.*, vol. 66, no. 4, pp. 352–355, 1998.

[21] P. Boucher. (2006, Oct.). *Points on a Sphere* [Online]. Available: http://www.softimageblog.com/archives/115

[22] C. R. Seubert and H. Schaub, "Electrostatic force model for terrestrial experiments on the coulomb testbed," in *Proc. 61st Int. Astron. Congr.*. Sep. 2010, no. IAC-10.C1.1.9.

[23] J. A. Soules, "Precise calculation of the electrostatic force between charged spheres including induction effects," *Amer. J. Phys.*, vol. 58, no. 12, pp. 1195–1199, 1990.

[24] C. Brebbia, *The Boundary Element Method for Engineers*. Mountain View, CA, USA: Pentech, 1978.

[25] W. C. Gibson, *The Method of Moments in Electromagnetics*, 1st ed. London, U.K.: Chapman & Hall, 2007.

[26] V. Davis and M. Mandell, "Plasma interactions with spacecraft," AFRL, Kirtland Air Force Base, NM, USA, Tech. Rep. AFRL-RV-PS-TR-2011-0089, vol. 2, Apr. 2011.

[27] R. F. Harrington, "Matrix methods for field problems," *Proc. IEEE*, vol. 55, no. 2, pp. 136–149, Feb. 1967.

Authors' photographs and biographies not available at the time of publication.